Inorg. Chem. **2002**, *41*, 5575–5581

Effect of Metal–Ligand Bond Lengths on Superexchange Interactions in Jahn–Teller d^4 Ion Systems: Spin Dimer Analysis of the Magnetic Structure of Marokite $CaMn_2O_4$

Myung-Hwan Whangbo,* Hyun-Joo Koo, and Dadi Dai

Department of Chemistry, North Carolina State University, Raleigh, North Carolina 27695-8204

Dongwoon Jung

Department of Chemistry, Wonkwang University, Iksan, Jeonbuk, South Korea 570−749

Received March 29, 2002

In marokite $CaMn_2O_4$, all six Mn–O bonds of each MnO_6 octahedron are different because of the Jahn–Teller distortion so that every Mn^{3+} (d^4) ion has six different superexchange interactions with its neighboring Mn^{3+} ions. The spin exchange interactions of $CaMn_2O_4$ were examined on the basis of spin dimer analysis to find what geometrical parameters of the Mn–O–Mn superexchange paths control the signs and strengths of their spin exchange interactions. Our work correctly describes the magnetic structure of $CaMn_2O_4$ observed from neutron powder diffraction measurements and shows that the antiferromagnetic interactions of the Mn–O–Mn paths depend primarily on the asymmetry and the Mn–O bond length of the Mn–O–Mn bridge, but not on the ∠Mn–O–Mn bond angle.

1. Introduction

In a magnetic solid of transition metal atoms M surrounded by main group elements L, the spin exchange interactions between adjacent metal atoms M can take place either through M−L−M superexchange paths or through M−L···L−M super-superexchange paths. In spin dimer analysis, the strengths of these spin exchange interactions are examined by performing electronic structure calculations for spin dimers (i.e., structural units consisting of two spin sites M and their surrounding ligands L). In the first-principles approach,[1−3] one calculates the energy differences between the high- and low-spin states of spin dimers to determine quantitatively the associated spin exchange parameters *J*. In the semiempirical approach,[4−11] one estimates the hopping integrals *t* between spin sites (i.e., half the spin orbital interaction energies Δ*e*) from molecular orbital (MO) calculations of spin dimers to extract trends in spin exchange interactions. In predicting whether a given M−L−M superexchange interaction is ferromagnetic (FM) or antiferromagnetic (AFM) without any electronic structure calculations, Goodenough rules[12−17] are employed. These rules predict the sign of an M−L−M superexchange (i.e., minus for AFM and plus for FM) on the basis of the ∠M−L−M bond angle, the symmetry properties of the metal d-orbitals containing unpaired spins, and the number of unpaired spins at the metal site M. These symmetry relations were first developed by Goodenough[12−14] and then extended by Kanamori[15] and Anderson.[16,17]

* To whom correspondence should be addressed. E-mail: mike_whangbo@ncsu.edu.

(1) Illas, F.; Moreira, I. de P. R.; de Graaf, C.; Barone, V. *Theor. Chem. Acc.* **2000**, *104*, 265 and references therein.
(2) Noodleman, L. *J. Chem. Phys.* **1981**, *74*, 5737.
(3) Dai, D.; Whangbo, M.-H. *J. Chem. Phys.* **2001**, *114*, 2887.
(4) Hay, P. J.; Thibeault, J. C.; Hoffmann, R. *J. Am. Chem. Soc*. **1975**, *97*, 4884.
(5) Kahn, O. *Molecular Magnetism*; VCH Publishers: Weinheim, 1993.
(6) Koo, H.-J.; Whangbo, M.-H. *J. Solid State Chem*. **2000**, *151*, 96.
(7) Koo, H.-J.; Whangbo, M.-H. *J. Solid State Chem*. **2000**, *153*, 263.
(8) Koo, H.-J.; Whangbo, M.-H. *Inorg. Chem*. **2000**, *39*, 3599.
(9) Koo, H.-J.; Whangbo, M.-H. *Inorg. Chem*. **2001**, *40*, 2169 and references therein.
(10) Dai, D.; Koo, H.-J.; Whangbo, M.-H. In *Solid State Chemistry of Inorganic Materials III*, MRS Symposium Proceedings; Geselbracht, M. J., Greedan, J. E., Johnson, D. C., Subramanian, M. A., Eds.; Materials Research Society: Warrendale, PA, 2001; Vol. 658, GG5.3.1-5.3.11 and the references therein.
(11) Koo, H.-J.; Whangbo, M.-H.; Coste, S.; Jobic, S. *J. Solid State Chem*. **2001**, *156*, 464.
(12) Goodenough, J. B. *Phys. Rev*. **1955**, *100*, 564.
(13) Goodenough, J. B. *J. Phys. Chem. Solids* **1958**, *6*, 287.
(14) Goodenough, J. B. *Magnetism and the Chemical Bond*; Wiley: Cambridge, MA, 1963.
(15) Kanamori, J. *J. Phys. Chem. Solids* **1958**, *6*, 287.
(16) Anderson, P. W. In *Magnetism*; Rado, G. T., Suhl, H., Eds.; Academic Press: New York, 1963; Vol. 1, Chapter 2.
(17) For the historical development of the concept of spin exchange interaction, see: Ginsberg, A. P. *Inorg. Chim. Acta, Rev*. **1971**, *5*, 45.

10.1021/ic0202458 CCC: $22.00
Published on Web 09/21/2002

Marokite $CaMn_2O_4$ [18,19] consists of high-spin Mn^{3+} (d^4) ions.[18] From a peak in the magnetic susceptibility, the appearance of symmetry-lowering magnetic Bragg reflections in neutron diffraction and the AFM long-range-ordered moment of $CaMn_2O_4$, it is clear that $CaMn_2O_4$ undergoes a three-dimensional (3D) AFM order below 220 K and has no spin frustration.[18] Goodenough rules are not clearly stated for magnetic solids made up of Jahn−Teller ions that exhibit a wide variation in the M−L bond lengths and the asymmetry of the M−L−M bridges. Trends in spin exchange interactions of various magnetic solids have been well described by the spin dimer analysis based on semiempirical molecular orbital calculations.[6−11] In the present work, we employ this method to analyze the magnetic structure of $CaMn_2O_4$, in which the Mn−O bond lengths and the asymmetry of the Mn−O−Mn bridges show a wide variation because of the Jahn−Teller distortion associated with the high-spin Mn^{3+} ions. Our work is organized as follows: In section 2, we discuss the geometrical parameters of the Mn−O−Mn paths and the signs of their superexchange interactions observed experimentally. In section 3, we discuss the method of spin dimer analysis relevant for magnetic solids consisting of metal ions with several unpaired spins. Results of our spin dimer analysis are presented and discussed in section 4. How the strengths of the calculated spin exchange interactions depend on the Mn−O bond lengths is discussed in section 5. Finally, the main conclusions of our work are presented in section 6.

2. Local Environments of Spin Sites and Observed Magnetic Structure

The building blocks of marokite $CaMn_2O_4$ are MnO_6 octahedra. All the Mn^{3+} ions are equivalent in $CaMn_2O_4$, but the Jahn−Teller distortion of each MnO_6 octahedron makes all six Mn−O bonds different [18,19] (e.g., 1.897, 1.910, 1.923, 1.958, 2.361, and 2.449 Å[13]). Thus, every Mn^{3+} ion has six different superexchange interactions with its neighboring Mn^{3+} ions (see later).[18] In these superexchange paths, the ∠Mn−O−Mn bond angles and Mn−O bond lengths vary widely.

It is convenient to consider $CaMn_2O_4$ as constructed from MnO_4 octahedral chains made up of trans edge-sharing MnO_6 octahedra (Figure 1a,b). The MnO_4 chains of $CaMn_2O_4$ run along the a-direction and share their edges and corners to form the 3D Mn_2O_4 lattice (Figure 1c),[18,19] whose triangular tunnels are occupied by Ca^{2+} ions. Note that the 3D Mn_2O_4 lattice can be viewed as constructed from layers of edge-sharing MnO_6 octahedra (parallel to the ab-plane) by sharing their octahedral corners (Figures 1c and 2a,b).

A perspective framework view of the Mn_2O_4 lattice is shown in Figure 2a, where the Mn sites labeled A through G were used by Ling et al.[18] to specify the six different superexchange interactions that a given Mn^{3+} site can have,

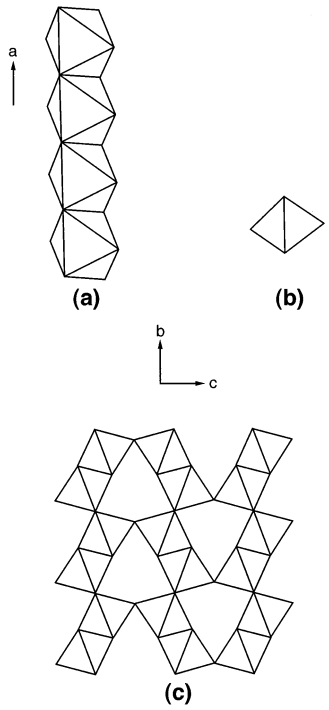

Figure 1. (a) Perspective view of an edge-sharing MnO_4 octahedral chain in polyhedral representation. (b) Projection view of an edge-sharing MnO_4 octahedral chain along the chain direction in polyhedral representation. (c) Projection view of the 3D Mn_2O_4 lattice of $CaMn_2O_4$ in polyhedral representation.

i.e., (A−B), (A−C), (A−D), (A−E), (A−F), and (A−G). Table 1 summarizes the geometrical parameters associated with these Mn−O−Mn superexchange paths (taken from the crystal structure of Ling et al.[18]). It is noted that the Mn−O−Mn bridges are symmetric in the paths (A−B) and (A−C), slightly asymmetric in the path (A−E), and highly asymmetric in the paths (A−D), (A−F), and (A−G). In addition, in the symmetric and nearly symmetric superexchange paths, the Mn−O bond lengths increase in the order (A−C) < (A−E) < (A−B).

Table 2 lists the signs of the six superexchange interactions determined by Ling et al.[18] from their powder neutron diffraction study. They also examined the signs of these interactions on the basis of Goodenough rules, and the result of their analysis is summarized in Table 2. The ∠Mn−O−Mn bond angle of the path (A−C) is 135.6°, which Ling et al. considered as lying in the transition zone between FM (angles close to 180°) and AFM (angles close to 90°) interactions, thereby concluding that the spin exchange of the path (A−C) is weak.[18] In the 3D Mn_2O_4 lattice, layers of edge-sharing MnO_6 octahedra (parallel to the *ab*-plane) are condensed by corner sharing to form the paths (A−C) (Figures 1c and 2a,b). Then, the preceding prediction implies that adjacent layers of edge-sharing MnO_6 octahedra can be coupled through the paths (A−C) either by FM or by AFM interactions, which is contrary to the observed 3D AFM ordering at a high temperature.

3. Spin Dimer Analysis

In understanding the anisotropy of spin exchange interactions of magnetic solids, it is often sufficient to estimate the

(18) Ling, C. D.; Neumeier, J. J.; Argyriou, D. N. *J. Solid State Chem.* **2001**, *160*, 167.
(19) Gieber, H. G.; Pennington, W. T.; Kolis, J. W. *Acta Crystallogr., Sect. C* **2001**, *57*, 329.

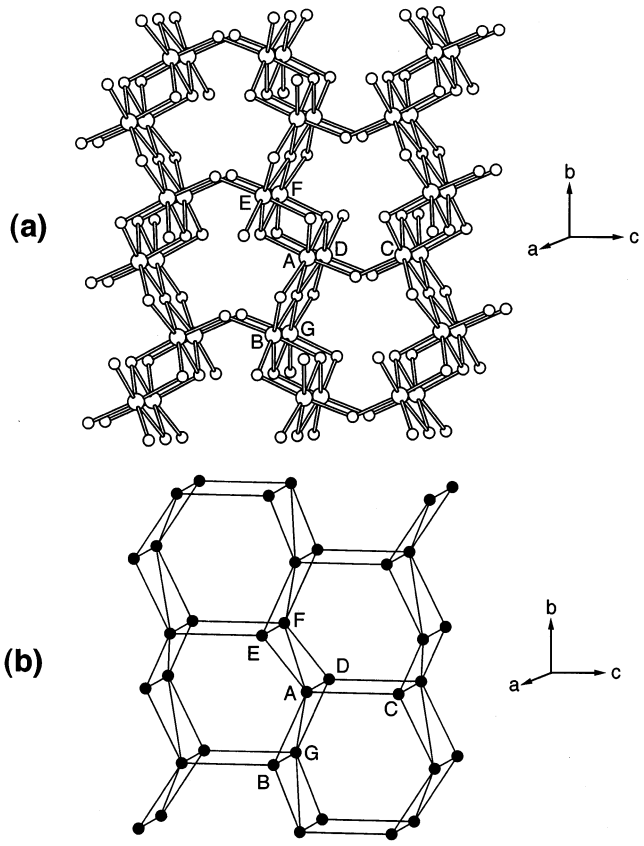

Figure 2. (a) Framework view of the 3D Mn_2O_4 lattice, where the Mn^{3+} sites labeled A through G are used to specify six different superexchange interactions (A−B), (A−C), (A−D), (A−E), (A−F), and (A−G) that a given Mn site can have. (b) Schematic view of the arrangement of the Mn atoms (●) in $CaMn_2O_4$.

Table 1. Geometrical Parameters Associated with the Six Mn−O−Mn Superexchange Paths of $CaMn_2O_4$[a]

interaction	bridging	Mn···Mn (Å)	Mn−O−Mn (Å)	∠Mn−O−Mn (deg)
(A−B)	edge	3.042	1.958/1.958	102.0
			2.445/2.445	76.9
(A−C)	corner	3.513	1.897/1.897	135.6
(A−D)	edge	3.147	2.361/1.923	94.0
			1.958/2.445	90.6
(A−E)	edge	2.903	1.910/1.923	98.4
			1.923/1.910	98.4
(A−F)	edge	3.194	2.361/1.910	96.2
			1.910/2.361	96.2
(A−G)	corner	4.377	1.958/2.445	167.5

[a] Taken from the crystal structure of ref 18.

Table 2. Signs of the Six Superexchange Interactions of $CaMn_2O_4$ Predicted by Goodenough Rules and Observed by Experiment

interaction	∠Mn−O−Mn (deg)	Goodenough rules[a]	expt[a]
(A−B)	102.0, 76.9	AFM	AFM
(A−C)	135.6	?	AFM
(A−D)	94.0, 90.6	AFM	AFM
(A−E)	98.4, 98.4	AFM	AFM
(A−F)	96.2, 96.2	?	FM
(A−G)	167.5	FM	FM

[a] Taken from ref 18.

relative magnitudes of their J values.[6−11] In general, a spin exchange parameter J is written as $J = J_F + J_{AF}$, where the FM term J_F (>0) is small so that the spin exchange becomes FM (i.e., $J > 0$) when the AFM term J_{AF} (<0) is negligibly small in magnitude. Thus, AFM spin exchange interactions (i.e., $J < 0$) can be discussed by focusing on the J_{AF} terms.

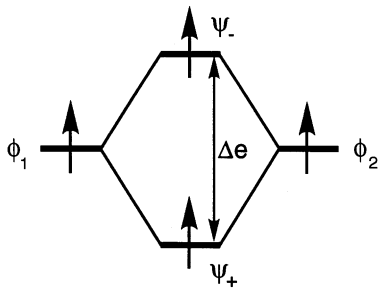

Figure 3. Spin orbital interaction energy Δe of a spin dimer with two equivalent spin sites.

Consider a spin dimer in which each spin site contains one unpaired electron, and the two spin sites are equivalent and represented by nonorthogonal magnetic orbitals (i.e., singly occupied molecular orbitals of the spin monomers) ϕ_1 and ϕ_2. Provided that S and Δe are, respectively, the overlap integral and the spin orbital interaction energy (Figure 3) between ϕ_1 and ϕ_2, then the J_{AF} term varies as $J_{AF} \propto -(\Delta e)^2 \propto -S^2$. When each spin site of a spin dimer has m unpaired spins, the overall spin exchange parameter J of the spin dimer is described by[5,20]

$$J = \sum_{\mu=1}^{m}\sum_{\nu=1}^{m}\frac{J_{\mu\nu}}{m^2} \tag{1}$$

From the viewpoint of nonorthogonal spin orbitals localized at the spin sites, the AFM contribution J_{AF} from each off-diagonal term $J_{\mu\nu}$ ($\mu \neq \nu$) is negligible because the overlap integral between two adjacent spin orbitals of different symmetry is either zero or negligible. Consequently, for AFM spin exchange interactions J, only the diagonal $J_{\mu\mu}$ terms can contribute significantly.[10,11,21]

$$J \approx \sum_{\mu=1}^{m}\frac{J_{\mu\mu}}{m^2} \tag{2}$$

Therefore, the AFM spin exchange parameters J can be related to the average of the spin orbital interaction energy squares $\langle(\Delta e)^2\rangle$,[10,11,21]

$$\langle(\Delta e)^2\rangle = \sum_{\mu=1}^{m}\frac{(\Delta e_{\mu\mu})^2}{m^2} \tag{3}$$

where $\Delta e_{\mu\mu}$ is the spin orbital interaction energy associated with the magnetic orbitals ϕ_μ of the two spin sites.

The spin orbital interaction energy $\Delta e_{\mu\mu}$ is related to the hopping integral t_μ between spin sites (i.e., the resonance integral between the magnetic orbitals ϕ_μ) by the relationship $\Delta e_{\mu\mu} \approx 2t_\mu$. In addition, the AFM component of the $J_{\mu\mu}$ term, $J_{\mu\mu,AF}$, is related to $\Delta e_{\mu\mu}$ and t_μ as follows[4,5,21,22]

(20) Charlot, M. F.; Kahn, O. *Nouv. J. Chim.* **1980**, *4*, 567.
(21) Whangbo, M.-H.; Koo, H.-J. *Inorg. Chem.* **2002**, *41*, 3570.
(22) This expression is valid when the strength of spin exchange interaction in a given exchange path is measured in units of J rather than in units of $2J$.

$$J_{\mu\mu,AF} = -\frac{4(t_\mu)^2}{U_{\text{eff}}} \approx -\frac{(\Delta e_{\mu\mu})^2}{U_{\text{eff}}} \quad (4)$$

where U_{eff} is the effective on-site repulsion, which should be constant for a given system. Therefore, if the average of the hopping integral squares is defined as

$$\langle t^2 \rangle \equiv \sum_{\mu=1}^{m} \frac{(t_\mu)^2}{m^2} \quad (5)$$

then $\langle (\Delta e)^2 \rangle \approx 4\langle t^2 \rangle$. Consequently, the AFM component of the overall spin exchange parameter J of the spin dimer is written as[21,22]

$$J_{\text{AF}} = -\frac{4\langle t^2 \rangle}{U_{\text{eff}}} \approx -\frac{\langle (\Delta e)^2 \rangle}{U_{\text{eff}}} \quad (6)$$

For spin dimers representing M−L−M superexchange interactions, the $\Delta e_{\mu\mu}$ values can be determined by performing MO calculations for the spin dimers. The corresponding hopping integrals t_μ are deduced indirectly from the relationship, $\Delta e_{\mu\mu} \approx 2t_\mu$.

For the case of $CaMn_2O_4$, the spin monomer (a structural unit consisting of a metal ion Mn^{3+} (d^4) plus its surrounding ligands O^{2-}) is given by $(MnO_6)^{9-}$ and has four magnetic orbitals. The spin dimers with a corner-sharing MnO_6 octahedra are given by $(Mn_2O_{11})^{16-}$, and those with an edge-sharing MnO_6 octahedra by $(Mn_2O_{10})^{14-}$. In describing the spin exchange interactions of magnetic solids in terms of Δe values obtained from extended Hückel MO calculations,[23,24] it is found necessary[6−11,21] to employ double-ζ Slater type orbitals[25] for both the 3d-orbitals of the transition metal and the s/p-orbitals of the surrounding ligand atoms. The atomic orbital parameters of Mn and O employed for our calculations are summarized in Table 3.[26,27]

4. Results and Discussion

4.1. Spin Exchange Interactions and Ordered Magnetic Structure. Table 4 summarizes the $\langle (\Delta e)^2 \rangle$ values calculated for the six superexchange paths of $CaMn_2O_4$ on the basis of the crystal structure of Ling et al.[18] Our calculations using the crystal structure of Gieber et al.[19] lead essentially to the same results and hence are not shown. The relative J_{AF} values of Table 4 were calculated using the largest $\langle (\Delta e)^2 \rangle$ value as the reference. According to these J_{AF} values, the strengths of the AFM interactions decrease in the order

$$(A-C) > (A-E) > (A-B) \gg (A-D) > (A-G) > (A-F) \quad (7)$$

from which we observe the following: (a) The weakest two AFM interactions occur in the paths (A−G) and (A−F), which are observed to be FM.[18] (b) The strongest AFM interaction occurs in the path (A−C), which is observed to be AFM.[18] (c) The extent of AFM interaction is strong in the paths (A−E) and (A−B) and is substantial in the path (A−D), all of which are observed to be AFM.[18] For our qualitative discussion, it is important to recall that a spin exchange parameter J becomes FM when the J_{AF} term is small in magnitude because the J_{F} term is small. Thus, the findings a−c are entirely consistent with the magnetic structure of $CaMn_2O_4$ determined by the neutron powder diffraction study.[18] Thus, the ordered magnetic structure of $CaMn_2O_4$ can be described as in Figure 4a,b. The three strongest AFM interactions (A−C), (A−E), and (A−B) form honeycomb sheets (Figure 4a,b) parallel to the *bc*-plane, and adjacent honeycomb sheets are coupled antiferromagnetically along the *a*-direction through the paths (A−D) (Figure 4a).

4.2. Qualitative Features of Spin Exchange Interactions. The strongest AFM interaction occurs in the path (A−C). In terms of spin orbital interaction energies Δe, it is straightforward to see why this path has a strong AFM interaction. The structure of the spin dimer representing the (A−C) interaction is depicted in Figure 5, where the lower-lying MnO_6 octahedron was oriented such that its Mn−O bonds are aligned along the Cartesian coordinate axes as close as possible. We classify the primary orbital character of the magnetic orbitals at each Mn^{3+} site with respect to the local coordinate of the lower-lying MnO_6 octahedron. Then, the Mn d-orbital symmetries of the four magnetic

Table 3. Exponents ζ_i and Valence Shell Ionization Potentials H_ii of Slater Type Orbitals χ_i Used for Extended Hückel Tight-Binding Calculation[a]

atom	χ_i	H_{ii} (eV)	ζ_i	C^b	ζ'_i	C'^b
Mn	4s	−9.75	1.844	1.0		
Mn	4p	−5.89	1.350	1.0		
Mn	3d	−11.67	5.767	0.3898	2.510	0.7297
O	2s	−32.3	2.688	0.7076	1.675	0.3745
O	2p	−14.8	3.694	0.3322	1.825[c]	0.7448

[a] H_{ii} values are the diagonal matrix elements $\langle \chi_i | H^{\text{eff}} | \chi_i \rangle$, where H^{eff} is the effective Hamiltonian. In our calculations of the off-diagonal matrix elements $H^{\text{eff}} = \langle \chi_i | H^{\text{eff}} | \chi_j \rangle$, the weighted formula was used. See: Ammeter, J.; Bürgi, H.-B.; Thibeault, J.; Hoffmann, R. *J. Am. Chem. Soc.* **1978**, *100*, 3686. [b] Contraction coefficients used in the double-ζ Slater type orbital. [c] References 21 and 27.

Table 4. $\langle (\Delta e)^2 \rangle$ and Relative J_{AF} Values Calculated for the Six Superexchange Interactions of $CaMn_2O_4$

interaction	$\langle (\Delta e)^2 \rangle^a$	relative $J_{\text{AF}}{}^b$
(A−B)	1028	0.40
(A−C)	2543	1.00
(A−D)	571	0.22
(A−E)	1827	0.72
(A−F)	170	0.07
(A−G)	301	0.12

[a] These values, presented in units of $(\text{meV})^2$, were calculated using the crystal structure of ref 18. [b] The path (A−C) was taken as the reference.

(23) Hoffmann, R. *J. Chem. Phys*. **1963**, *39*, 1397.
(24) Our calculations were carried out by employing the *CAESAR* program package (Ren, J.; Liang, W.; Whangbo, M.-H. *Crystal and Electronic Structure Analysis Using CAESAR*; http://www.PrimeC.com/, 1998).
(25) Clementi, E.; Roetti, C. *Atomic Data Nucl. Data Tables* **1974**, *14*, 177.
(26) The diffuse exponent ζ' of the O 2p-orbital is larger (i.e., more contracted) than the atomic value reported in ref 21 by 10%. Our studies on magnetic oxides Cu_4O_3 (ref 21) and $(VO)_2P_2O_7$ (ref 27) show that the ζ' value of O 2p appropriate for the study of spin exchange interactions should be larger than the atomic value of ref 25 by 10−13%.
(27) Koo, H.-J.; Whangbo, M.-H.; VerNooy, P. D.; Torardi, C. C.; Marshall, W. J. *Inorg. Chem*. **2002**, *41*, 4664.

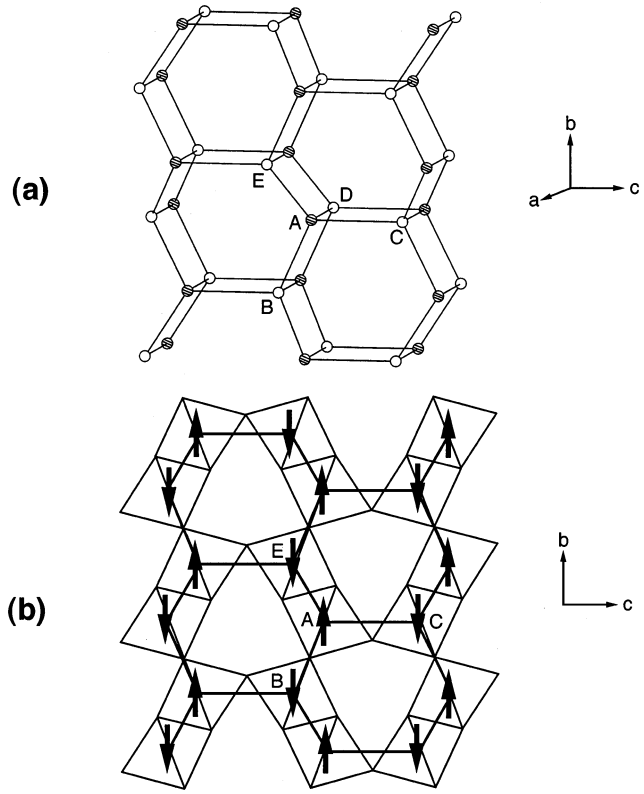

Figure 4. (a) Schematic view of the ordered spin arrangement in the 3D Mn_2O_4 lattice of $CaMn_2O_4$, where shaded and open circles represent up-spin and down-spin Mn sites, respectively. (b) Schematic view of the AFM arrangement of spins within a honeycomb sheet by using the projection view of the lattice shown in Figure 1c.

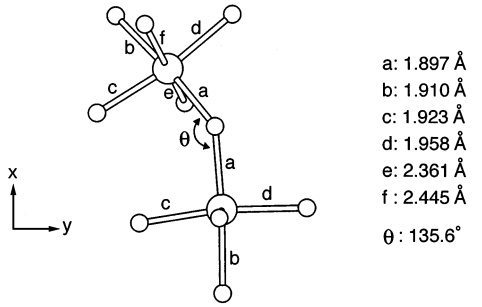

Figure 5. Arrangements of the Mn−O bonds in the spin dimer representing the superexchange path (A−C). The six Mn−O bonds of the lower-lying MnO_6 octahedron are aligned along the Cartesian coordinate axes as close as possible (i.e., the bonds b/a along the *x*-direction, the bonds c/d along the *y*-direction, and the bonds f/e along the *z*-direction).

orbitals are *xz*, *xy*, *yz*, and z^2. Note that the Mn−O−Mn bridge of this spin dimer is symmetric and is made up of the shortest Mn−O bonds. Consequently, two of the four magnetic orbitals (i.e., "*xz*" and "*xy*" orbitals) on each spin site give rise to two strong π-type orbital interactions through the Mn−O−Mn bridge (Figure 6a,b).[28] In each π-type orbital interaction, the 2p-orbital of the bridging oxygen is absent in the lower level ψ_+ by symmetry but contributes strongly out-of-phase to the Mn 3d-orbitals in the upper level ψ_- because the Mn−O−Mn bridge is symmetric and because the Mn−O bonds are short (i.e., Mn−O = 1.897/1.897 Å, Table 1). Consequently, the energy split between the ψ_+ and

(28) Whangbo, M.-H.; Canadell, E. *Acc. Chem. Res.* **1989**, *22*, 375.

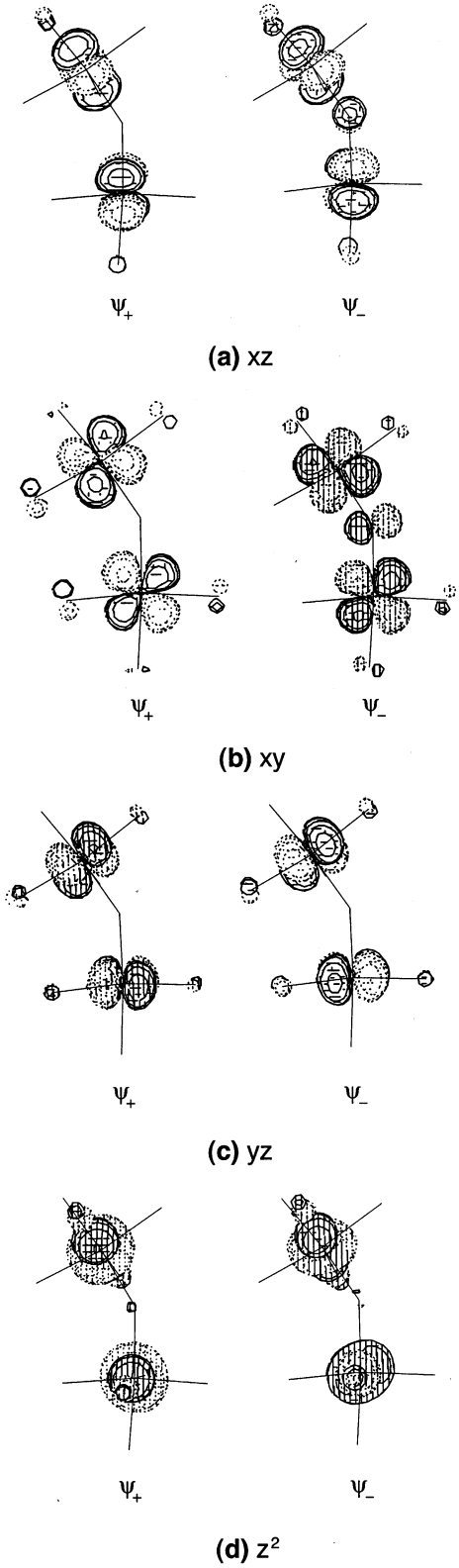

Figure 6. Pairs of the singly occupied molecular orbitals ψ_+ and ψ_- defining the spin orbital energies Δe in the spin dimer representing the superexchange path (A−C). In parts a−d, the symmetries of the magnetic orbitals at the spin sites were classified with respect to the d-block orbitals of the lower-lying MnO_6 octahedron in the spin dimer.

ψ_- levels (i.e., the spin orbital interaction energy Δe) is large for the "*xz*" and "*xy*" magnetic orbitals. The remaining two magnetic orbitals (i.e., "*yz*" and "z^2" orbitals) of each spin

site lead to a negligible Δe because the 2p-orbital of the bridging oxygen cannot contribute to both ψ_+ and ψ_- by symmetry (Figure 6c) and because the 2p-orbital of the bridging oxygen contributes very weakly to both ψ_+ and ψ_- by orbital mismatch (Figure 6d). Because of the two strong π-type orbital interactions, the spin exchange path (A−C) becomes strongly AFM.

The second strongest AFM interaction occurs in the path (A−E), where the two Mn−O−Mn bridges are only slightly asymmetric (Mn−O = 1.910/1.923 Å) and the bridging Mn−O bonds are relatively short. The third strongest AFM interaction occurs in the path (A−B), in which both Mn−O−Mn bridges are symmetric, and the bridging Mn−O bonds are relatively long (Mn−O = 1.958/1.958 Å) in one bridge and very long in another bridge (Mn−O = 2.445/2.445 Å). The decrease in the strength of the AFM interaction in the order (A−C) > (A−E) > (A−B) is readily explained by considering that the extent of a π-type orbital interaction through a symmetric (or nearly symmetric) Mn−O−Mn bridge decreases with increasing the Mn−O bond length.

The fact that the paths (A−F) and (A−G) are FM, i.e., their AFM interactions are very weak, can be easily understood because the Mn−O−Mn bridges are strongly asymmetric [e.g., Mn−O = 1.910/2.361 Å in the path (A−F) and Mn−O = 1.958/2.445 Å in the path (A−G)] so that the energy split between the ψ_+ and ψ_- levels becomes very small for each magnetic orbital. The two Mn−O−Mn bridges of the path (A−D) are quite asymmetric as well (i.e., Mn−O = 1.923/2.361 Å; 1.958/2.445 Å), so the extent of AFM interaction in the path (A−D) would be weak. On the basis of inspecting the asymmetry of the Mn−O−Mn bridges alone, it is impossible to predict if the AFM interaction of the path (A−D) will be as weak as those of the paths (A−F) and (A−G). Certainly, calculations of $\langle(\Delta e)^2\rangle$ allow one to estimate the relative strengths of such interactions.

5. Effect of the M−L Bond Lengths on the Spin Exchange Interactions of a Jahn−Teller d^4 Ion System

For a system made up of Jahn−Teller ions (e.g., d^4 ions), a strong variation occurs in the M−L bond lengths and in the asymmetry of the M−L−M bridges. Thus, in understanding the spin exchange interactions of such a system, it is necessary to examine the role of M−L bond lengths in determining the strength of superexchange interaction. With respect to the local coordinate axis defined in Figure 6, the magnetic orbitals associated with each Mn^{3+} (d^4) ion site have the *xz*, *xy*, *yz*, and z^2 symmetries. The *xz*, *xy*, and *yz* orbitals originate from the t_{2g} set, and the z^2 orbital from the e_g set. The z^2 orbital has its principal orbital lobes aligned along the long Mn−O bonds. The x^2-y^2 orbital of an Mn^{3+} ion site is unoccupied (hence not shown) and has its orbital lobes aligned along the short Mn−O bonds. In principle, there are 16 possible combinations of orbital interactions between two adjacent Mn^{3+} (d^4) sites (eq 1). According to the approximation leading from eq 1 to eq 2, only the four diagonal combinations can have strong AFM interactions (i.e., *xz*/*xz*, *xy*/*xy*, *yz*/*yz*, and z^2/z^2). It is convenient to consider the superexchange interactions associated with Jahn−Teller d^4 ions for three different cases of M−L−M bridges.

5.1. Symmetric M−L−M Bridges of Short M−L Bonds. Examples of this case are the (A−C), (A−E), and (A−B) interactions discussed in section 4. As already described, only two of these four diagonal combinations (i.e., *xz*/*xz* and *xy*/*xy*) have strong AFM interactions. These two combinations, which have π-interactions across the Mn−O−Mn bridge (Figure 6a,b), arise from two of the three t_{2g} set orbitals. The remaining t_{2g} orbital (i.e., *yz*) cannot provide AFM interactions because it leads to δ-interactions across the Mn−O−Mn bridge (Figure 6c). For a Mn−O−Mn bridge consisting of short Mn−O bonds, the e_g set orbital z^2 cannot give rise to AFM interactions because this orbital is oriented along the long Mn−O bonds (i.e., perpendicular to the short Mn−O bonds) thereby leading to negligible overlap interactions between the two z^2 orbitals (Figure 6d). This analysis reveals that the signs of M−L−M superexchange interactions for a Jahn−Teller d^4 system are determined primarily by the t_{2g} set orbitals if the M−L−M bridge is symmetric (or nearly symmetric) and is made up of short M−L bonds. Thus, all (A−C), (A−E), and (A−B) interactions of $CaMn_2O_4$ are predicted to be AFM. The strength of the AFM interaction should increase with shortening the M−L bond length and increasing the ∠M−L−M bond angle to 180°, but the bond length variation is more important than the bond angle variation. For example, the strengths of the AFM interactions in the (A−C), (A−E), and (A−B) paths in $CaMn_2O_4$ decrease in the order (A−C) > (A−E) > (A−B).

5.2. Symmetric M−L−M Bridges of Long M−L Bonds. This case does not occur in $CaMn_2O_4$. When the M−L bonds are long in a symmetric M−L−M bridge, the two π-interactions across the M−L−M bridge originating from two t_{2g} orbitals will be weak. The singly occupied e_g orbital (i.e., the z^2 orbital in Figure 6) will have its orbital oriented along the long M−L bond. This will give rise to a substantial σ-interaction, and hence a substantial AFM interaction, across the M−L−M bridge.

5.3. Asymmetric M−L−M Bridges of Long and Short M−L Bonds. The (A−D), (A−F), and (A−G) interactions discussed in section 4 are examples of this case. In general, π-interactions across an M−L−M bridge become weak when the bond length asymmetry of the bridge is large. Thus, for a strongly asymmetric M−L−M bridge, the π-interactions arising from the t_{2g} orbitals would be weak. The singly occupied e_g orbital (i.e., z^2) is aligned along the long M−L bond. Therefore, in an asymmetric M−L−M bridge, one z^2 orbital is aligned along the long M−L bond while the other z^2 orbital is aligned along a direction perpendicular to the short M−L bond. Thus, the two magnetic orbitals arising from the two e_g orbitals will have a negligible overlap across the M−L−M bridge and hence will lead to a negligibly weak antiferromagnetic interaction. Consequently, the orbital interactions between the metal centers in a highly asymmetric M−L−M superexchange path will be weak, and hence, the superexchange interaction is most likely FM, as found for (A−F) and (A−G). However, the interaction may become

weakly AFM, as found for (A−D). Unless electronic structure calculations such as those described in our study are carried out, it would be difficult to predict if the interaction through a highly asymmetric M−L−M superexchange path would be FM or AFM.

6. Concluding Remarks

The trends in the $\langle(\Delta e)^2\rangle$ values calculated for the six superexchange paths of $CaMn_2O_4$ are entirely consistent with the observed magnetic structure of $CaMn_2O_4$.[18] From the present and other studies of magnetic solids,[6−11,21,27] it is evident that the relative strengths of M−L−M superexchange interactions are well described by $\langle(\Delta e)^2\rangle$. When each metal site M has several unpaired spins, the value of $\langle(\Delta e)^2\rangle$ is given by the average of several $(\Delta e_{\mu\mu})^2$ terms. The magnitude of each $\Delta e_{\mu\mu}$ depends on the ∠M−L−M bond angle as well as on the asymmetry and the average M−L bond length of the M−L−M bridge. In the six superexchange paths of $CaMn_2O_4$, the Mn−O bond lengths vary in a wide range. Consequently, the strengths of their spin exchange interactions are governed mainly by the asymmetry and the average Mn−O bond length of the Mn−O−Mn bridges, but not by the ∠Mn−O−Mn bond angle. Our analysis of the superexchange interactions of Jahn−Teller d^4 ion systems indicates that for a symmetric (or nearly symmetric) bridge made up of short M−L bonds, the superexchange interaction is expected to be AFM. For a symmetric (or nearly symmetric) bridge made up of long M−L bonds, the superexchange interaction is expected to be AFM. For a strongly asymmetric bridge made up of long and short M−L bonds, the superexchange interaction is most likely FM but can be weakly AFM.

Acknowledgment. The work at North Carolina State University was supported by the Office of Basic Energy Sciences, Division of Materials Sciences, U.S. Department of Energy, under Grant DE-FG02-86ER45259. D. Jung thanks Korea Research Foundation for the financial support under Grant DP0300. The authors are grateful to the reviewers for their critical and constructive comments, which were essential in revising the work.

IC0202458